CrossMark

# Metastatic breast cancer cells adhere strongly on varying stiffness substrates, initially without adjusting their morphology

Sonbula Massalha[1] · Daphne Weihs[1]

**Abstract** We show that metastatic breast cancer cells are quantitatively identifiable from benign cells during adherence onto soft, elastic gels. We identify differences in time-dependent morphology and strength of adherence of single breast cells that are likely related to their malignancy and metastatic potential (MP). Specifically, we compare high and low MP breast cancer cells with benign cells as a control on collagen-coated, polyacrylamide gels with Young's modulus in the physiological range of 2.4–10.6 kPa. We observe that the evaluated metastatic breast cancer cells remain rounded, with small contact area, up to 6.5 h following seeding. In contrast, the benign cells spread and become more elongated on stiffer gels. We identify measurable differences in the two-dimensional, lateral, traction forces exerted by the cells, where the rounded, metastatic cells apply significantly larger, traction forces, as compared to the benign cells, on gels stiffer than 2.4 kPa. The metastatic cell lines exhibited gel-stiffness-dependent differences in traction forces, strain energies, and morphologies during the initial stages of adhesion, which may relate to their MP or invasiveness.

**Keywords** Mechanobiology · Cell adherence · Traction force microscopy · Fluorescence microscopy · Metastatic potential

✉ Daphne Weihs
daphnew@technion.ac.il

1 Faculty of Biomedical Engineering, Technion-Israel Institute of Technology, 3200003 Haifa, Israel

## 1 Introduction

Cancer metastasis is the leading cause of death in cancer patients, with over 90% of cancer fatalities related to the spreading of the tumor cells to metastatic sites (Christofori 2006). Interactions between cancer cells and their microenvironment, such as adhesion, regulate the combined biochemical and mechanical processes that facilitate metastatic invasion. This study is focused on the initial stages of cell adhesion prior to cell morphology stabilization, showing significant differences between the evaluated metastatic-cancer and benign cell lines, as well as between the cells with varying metastatic potential. In the past few decades, the likelihood for metastases has been indicated through changes in biological markers (Sidransky 2002), gene expression, and more recently through mechanical interactions between the cells and the cancer microenvironment (Lelievre et al. 1998; Paszek and Weaver 2004). However, there are still no definite procedures to determine the for metastatic potential (MP) of cells and predict the likelihood for metastasis and more so to forecast the target organ (Kraning-Rush et al. 2012), leading to grim prognoses for metastatic cancer patients. Typically, to deliver prognosis and decide on clinical procedures and treatments, oncologists rely on pathological reports and statistical history of a specific cancer type to determine the metastatic phenotype of a tumor (Ravdin et al. 2001). Recently, we and others have shown that highly metastatic breast cancer cells are softer both externally and internally, as compared to non-metastatic cancer and benign breast cells (Guck et al. 2005; Cross et al. 2007; Gal and Weihs 2012); that relates to differences in cytoskeleton dynamics and internal structure of the cells (Mierke et al. 2010; Goldstein et al. 2013). Remarkably, we also showed that the same metastatic cells are also adaptable and were able to modify their cytoskeleton and morphology (Dvir et al. 2015) and apply strong mechani-

cally invasive forces to their microenvironment (Mierke et al. 2008; Kristal-Muscal et al. 2013, 2015). However, while these mechanical markers show great promise, they are not yet applicable as reliable tools to identify and classify cancer cells. Hence, determining the specific mechanical interactions of metastatic cancer cells with their microenvironment can lead to development of novel approaches to predict the likelihood for metastasis, as well as reveal mechanisms and stages of metastatic invasion.

Mechanical interactions of cancer cells with their microenvironment have revealed differences between cells with varying MP, albeit by focusing on the migration of cells and the late stages of metastasis formation (Kraning-Rush et al. 2012; Peschetola et al. 2013). Recently, the mechanical interactions of single cancer cells with their microenvironment have been evaluated following stabilization of the adhesive interactions (i.e., 24 h after seeding) and have been directly correlated with the cells' invasiveness and its MP (Zaman et al. 2006; Kristal-Muscal et al. 2013; Mak et al. 2013). Specifically, the ability of cells to change shape, modify their internal structure (cytoskeleton and nucleus), alter adhesion and migratory states is directly correlated with their ability to invade surrounding tissue. Tumor initiation (Vermolen et al. 2015) and invasion of metastatic cancer cells includes several stages combining mechanical and biochemical interactions. The focus of our work is on the initial stages of cell adhesion, which typically occur as cells migrate into new environments. For example, adhesion is an important stage of the transmigration of a cell through the endothelium of a blood vessel when extravasating into a potential, secondary tumor site (Mierke et al. 2008).

Cell adhesion is a time- and environment-dependent process consisting of two main stages: attachment and spreading. Those are, respectively, mainly biochemical and a combination of biochemical and biomechanical processes, part of a complex mechanobiology cascade. Biochemical signals from the extracellular matrix allow cancer cells to respond to changes in their microenvironment (Kumar and Weaver 2009). Cell interactions with their environment occurs through adhesion receptors (Bershadsky et al. 2003), and focal adhesions (Ingber 2008) by utilizing the cytoskeleton networks. Following initial attachment by biochemical connections, coordinated processes including the membrane molecules and the dynamically active cytoskeleton can modify cell structure and morphology to allow cell spreading and strengthening of cell-substrate connections; the cytoskeleton and especially its molecular motors facilitate dynamic remodeling and allow active transport and force generation within the cell. Although mechanical processes are critical in cell adhesion and invasion, cancer research has mostly been focused on the biochemistry of cell attachment and spreading (Paszek et al. 2005). Moreover, the mechanical processes that control cancer cell invasion, such as cell adhesion, cell

migration, changes in the cell shape, and the generation of forces, are currently not well understood. Thus, the focus of the current work is on evaluating the mechanical interactions of cells, specifically during the early stages of adhesion, likely before cells reach a stable morphology. This can shed light on important stages in the metastasis process revealing potentially prognostic differences between cells with varying MP.

From another perspective, it has been shown that the stiffness of the ECM and the cell microenvironment can have profound mechanical effects on the cell, such as changes in its morphology, motility, protein expression, and force generation (Lo et al. 2000; Discher et al. 2005; Yeung et al. 2005; Geiger and Yamada 2011). Focusing on the latter, previous studies showed that fibroblasts and endothelial cells (noncancerous) develop a flatter morphology on stiffer substrates (>3 kPa) and that cells will preferentially migrate from a soft to a stiff substrate (Discher et al. 2005; Yeung et al. 2005). Those mechanical effects alter with different cell types, and their response to the microenvironment. Cells respond to substrate rigidity cues by exerting actomyosin contractility (Ruppender et al. 2010), through integrins, focal adhesions, and the cytoskeleton (Rape et al. 2011); focal adhesion formation and actomyosin contractility are essential for cell adhesion to substrates (Pelham and Wang 1997). Specifically for cancer cells, the substrate rigidity regulates invasiveness at the primary site (Pelham and Wang 1997; Lo et al. 2000; Paszek et al. 2005; Levental et al. 2009), thus understanding the role of cell–ECM interactions and how the stiffness of the microenvironment affects the mechanical behavior of the cells is crucial for cancer diagnosis and early determination of the metastatic potential of a single cancer cell. Cancer cells exhibit altered tensional homeostasis, as compared to normal, nonmalignant cells and are thus expected to differ in contractility and spreading. Mammary epithelial cells evaluated on soft substrates (0.2–10 kPa) have shown higher contractility and larger cell spreading area than nonmalignant cells (Butcher et al. 2009; Kraning-Rush et al. 2012); in those works, measurements were taken at extended times after stabilization of cell morphology, unlike the measurements performed in the current work.

Here, we identify and evaluate differences in mechanical interactions of metastatic cells during the early onto stages of adherence, i.e., attachment and initial spreading onto varying stiffness gels. Those early interactions (up to 6.5 h following seeding) are likely related to the MP of the cells. Specifically, we have measured the time-dependent, two-dimensional (2D), traction forces applied laterally at the gel surface (Butler et al. 2002; Abuhattum et al. 2015) by breast cancer cells with different MP, as compared to a benign control, during adhesion to varying stiffness polyacrylamide (PAM) gels (Young's moduli of 2.4, 4.3, 7.2,

or 10.6 kPa), starting at 0.5 h and up to 6.5 h after seeding.

We show that both high and low MP cells apply significantly larger traction forces during adhesion as compared to the benign breast cells on all gels with Young's modulus larger than 2.4 kPa; on lower stiffness gels, traction forces applied by the cell lines were indistinguishable. Between the two evaluated metastatic cell lines, we observe gel-stiffness-dependent differences that may relate to their metastatic potential and the resulting invasiveness. Concurrently, the metastatic cancer cells remained mainly rounded, while benign cells became elongated with time, especially on the stiffest gels. These findings show a correlation between the MP of the adhering breast cancer cells and their small areas combined with the large mechanical forces applied by the cells, which is likely what facilitates their metastatic capabilities.

## 2 Materials and methods

### 2.1 Cell culture

Human epithelial breast cancer cell lines with high metastatic potential, MDA-MB-231 (HTB-26D, ATCC) and low MP, MDA-MB-468 (HTB-132, ATTC, Manassas, VA) were cultured in Dulbecco's modified Eagle's medium (DMEM, Gibco-Invitrogen, Carlsbad, CA); the relative metastatic potential of the two cell types had previously been reported (Cooney et al. 2011). The medium was supplemented with: 10% fetal bovine serum (FBS), 1% penicillin, 1% L-Glutamine, and 1% 1 mM Sodium pyruvate (all from Biological Industries, Kibbutz Beit Haemek, Israel). The benign epithelial breast cell line MCF 10A (CRL-10317, ATTC, Manassas, VA) was grown in 1:1 ratio of DMEM:F-12 media (Biological Industries, Kibbutz Beit Haemek, Israel), supplemented with 5% horse serum, 0.05% Hydrocortisone 1 mg/ml, 0.01% Cholera toxin, 0.1% Insulin at 10 mg/ml (all from Sigma-Aldrich, Rehovot, Israel), 1% penicillin streptomycin, and 1% L-Glutamine (both from Biological Industries, Kibutz Beit Haemek, Israel). The media was sterile filtered (0.2 µm pores), and then 0.01% human endothelial growth factor (EGF, Peprotech Asia, Rocky Hill, NJ) was added. All cell lines were cultured in a humidified incubator at 37 °C containing 5% $CO_2$ and were used at passages 10–30 from stock.

### 2.2 Gel preparation

Polyacrylamide (PAM) gels were prepared according to an established protocol (Raupach et al. 2007; Kristal-Muscal et al. 2013; Dvir et al. 2015), on a glass cover slip, No. 5 thickness, 30 mm diameter (Menzel, Germany). The glass surface

was first sterilized using 0.1M NaOH and then activated using 3-aminopropyltriethoxysilane (APTS, both Sigma-Aldrich, St. Louis, MO) and glutaraldehyde. Fluorescent beads, 2 µm in diameter, were glued (by drying) on the glass, where the fixed positions of the beads facilitate image dedrifting due to any mechanical drift with time. The PAM gels were formed by combining the monomers with distilled water according to the recipes provided in Online Resource 1. Fluorescent, carboxylated 200-nm diameter beads (Invitrogen, Carlsbad, CA) were added to the monomer solution. Gelation was initiated with ammonium persulfate (APS) and catalyzed with the tertiary aliphatic amine N,N,N′,N′-tetramethylethylenediamine (TEMED, both Sigma-Aldrich, St. Louis, MO). Solutions for gel preparation were kept at 4 °C and were mixed on ice to reduce the polymerization rate. Gels were prepared within a plastic frame (GeneFrame, 25 µl, 10 × 10 mm, ABgene Thermo-Scientific, Waltham, MA) stuck on the glass coverslip and covered with a flexible, plastic coverslip; gels were closed as oxygen inhibits polymerization. Gelation was performed while cooling to 2 °C and centrifuging for 30 min at 300$g$, to bring the beads to the gel surface (Raupach et al. 2007) and were left upside-down at room temperature for 2 h; the polymerization time was determined by rheology. Following polymerization, the gels were rinsed with HEPES pH 8.5 (Sigma, St Louis, MO) and kept in phosphate buffered saline. For this study, we used four substrates with different Young's moduli varying between 2 and 11 kPa (See Online Resource 1), within the physiological range of soft tissue stiffness (Levental et al. 2007). After full polymerization, the plastic coverslip is removed and the gel surface is activated with sulfo-SANPAH (Ornat, Israel) by UV light exposure, twice for 10 min each. After UV exposure, the gels are rinsed with HEPES for 15 min on a shaker, and this process is repeated twice. To allow cell adherence, the cells were coated with collagen solution (Rat tail type 1, Sigma, St. Louis, MO) which is added to the gels and left for 24 h at 4 °C. The collagen solution is replaced with PBS, and gels are kept at 4 °C for 12 h. Prior to cell seeding, PBS is replaced with media and gels are kept in an incubator for 1 h before use.

### 2.3 Gel stiffness

The Young's modulus of the gel was determined using a TA Instruments AR-G2 rheometer (New Castle, Delaware) with a 20 mm diameter parallel plate fixture. Gels were prepared on the rheometer plate, and the shear modulus ($G^*$) was measured during and after polymerization. Temperature was maintained at 37 °C throughout the measurement, to match the cell-experiment conditions. Sample evaporation and dehydration were minimized by placing water-droplets on the rheometer bottom-plate near the gel. Using strain and frequency sweeps, we determined that gels were elas-

tic ($G' >> G''$), and the Young's moduli ($E$) were thus obtained through: $E = 2G'(1 + \nu)$ where $\nu$ is the Poisson's ratio with a value of 0.48 for PAM gels (Boudou et al. 2009). The Young's modulus was varied between 2 and 11 kPa (see Online Resource 1 and Online Resource 2). The generated gels exhibit linear elastic responses up to at least 80% strain (not shown).

## 2.4 Sample preparation and image acquisition

Cells were seeded on the gel at a concentration (30,000 cells in 2mL growth media) that was optimized to image a single cell per field-of-view (FOV). Imaging was done using an Olympus IX81 inverted, epifluorescence microscope with on-stage humidified incubator maintaining 37 °C, 5% $CO_2$, and 90% humidity, and using a 60×/0.7NA differential interference contrast (DIC, Nomarsky Optics) air-immersion objective. Images were acquired using an XR Mega-10AWCL camera (Stanford Photonics Inc., Palo Alto, CA), at a final magnification of 107.8 nm/pixel. The cells were imaged every 1 h starting from 0.5 h after seeding up till 6.5 h, at randomly selected FOVs where cells were observed at the shortest time. For each cell type and each gel stiffness, we evaluated 15–20 cells. Three images were acquired at each time point in each FOV: (a) DIC image of the cells on the gel, (b) fluorescent image of the 200-nm diameter particles embedded at the gel surface, and (c) a fluorescent image of the 2 μm diameter particles on the glass cover slip, under the gel. At the end of each experiment, the cells were removed using trypsin (Solution C EDTA 0.02%, Biological Industries, Kibutz Beit Haemek, Israel), and images of the undeformed gel were obtained for each FOV.

## 2.5 Traction force microscopy

Bead displacements at the 2D gel surface were determined at each time point, relative to the undeformed gel following cell removal, and in-plane traction forces were calculated (Butler et al. 2002); traction force microscopy algorithms were kindly provided by Ramaswamy Krishnan, Harvard University. Figure 1 schematically shows the flow of the experiment and analysis procedures for calculating the displacement and stress maps. Briefly, bead positions were cross-correlated between the fluorescent images of the 200-nm beads, with and without the cell, using a sliding window of 32 × 32 pixels; the images were initially corrected for any local drift in the system using the positions of the large, fixed beads. That provided the displacement map of the current FOV at the specific time point. Using the displacement field and with the gel Young's modulus (i.e., stiffness) and its Poisson's ratio, we calculated the traction forces. Traction forces were confined to within the cell boundary only, and all forces outside the boundary were zeroed using an itera-

tive Fourier transform calculation; the cell boundaries were manually marked using custom codes in MATLAB 2012b (MathWorks, Nattick, MA), assuming that forces are only applied at a cell's location. We focus on the total traction force, which is the sum of the magnitudes (nondirectional) of the traction stresses vectors ($T$) applied over the entire cell area, $A$ : $F_{\text{total}} = \int\int \left|\vec{T}(\vec{r})\right| dA$. The total traction force is typically considered as the force applied at all focal adhesions, or the overall force production of the cell (Abuhattum et al. 2015; Soine et al. 2015).

## 2.6 Local force maxima analysis

Biological variability causes each cell to apply a wide range of traction force and strain energy magnitudes at different times, and each cell exhibited a different time evolution (Online Resource 3). The adhesion is experimentally monitored (imaged) at discrete, predetermined time points. Hence, an approach to normalize the timescales of each cell within its experiment is required. We observe that each of the single cells applies increasing and decreasing forces, which for each cell occur at different times during the adhesion process. This is a result of the different dynamics of each cell, and thus averaging over all the cells provides only partial information, and in many cases will mask the single cell dynamics; averaging is still appropriate in some cases and for some of the parameters. Thus, in cases of large changes with time we define the local maxima of the total forces applied by each cell, as demonstrated in Online Resource 4a (Kristal-Muscal et al. 2013). The local maxima of the total force indicate changes in cell-applied forces during interaction with the substrate. Online Resource 4b shows that the distribution of number of local force maxima during the experiment is independent of cell type. Thus, the number of force maxima is an independent parameter in our system, effectively providing a cell-normalized time; the first maximum always occurs at the shortest times, albeit different for each cell.

## 2.7 Cell morphology analysis

To quantitatively evaluate the morphological changes of the cells during adhesion, we determine the cell area and perimeter and then calculate the cells' eccentricity and circularity (Xiong et al. 2010; Ren et al. 2015); see Online Resource 5. Using a custom MATLAB module, we have manually marked the cell edge locations on the DIC images, and using that we automatically calculated the cell area and perimeter. Cell circularity, a measure of the relative smoothness of the cell perimeter (its 2D shape), is defined by $c = 4\pi A/p^2$, where $A$ and $p$ are the cell area and perimeter, respectively. The circularity values are between 0 and 1, where a circularity of 1 indicates a smooth edge, or cell boundary (Online
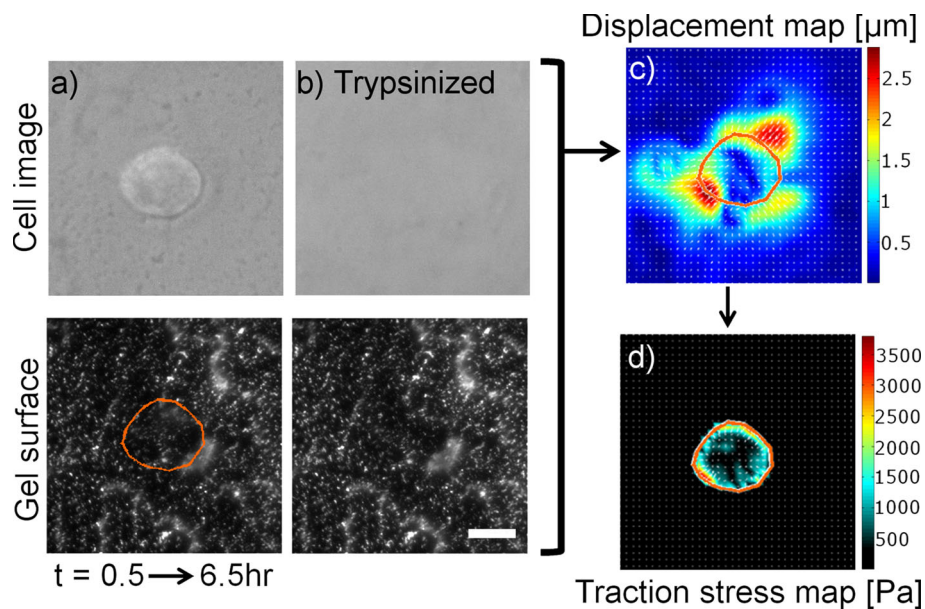
**Fig. 1** Traction force microscopy experiments. **a** Cells are seeded on a PAM gel (*top*) which has fluorescent beads embedded in its surface (*bottom*); the *orange line* is the cell boundary. Cell is imaged every 1 h after seeding, and gel deformations due to cell-applied forces are identified through beads displacement. **b** The cell is removed from the gel with trypsin, providing the undeformed, relaxed gel, reference state. **c** The displacement map of the beads between the cell-deformed and relaxed gel is calculated for each time point; **d** traction stress map is calculated from the displacement map by using the gels' Young's modulus and Poisson's ratio. *Scale bar* is 20 $\mu$m

Resource 5). Smaller values of the circularity indicate irregular edges, e.g., blebs, where in cells very low values may result from existence of many protrusions and lamellipodia. We have also determined the cell eccentricity, a measure of the relative elongation of the cells' shape, by approximating the cell shape to an ellipse with the same second-moments. The eccentricity is then given by the ratio of the distance between the foci of the ellipse and its major axis length. The eccentricity ranges between 0 and 1, respectively, indicating a circular shape or a line segment shape; the eccentricity of a spindle-shaped cell will be lower than unity.

### 2.8 Statistical analysis

Statistical analysis was performed to compare between the cell types on each gel stiffness. At all stiffness other than 2.4 kPa, differences in the cell lines were determined as significant using a two-way ANOVA with a post hoc Tukey test or a corrected Tukey–Kramer test; significance was determined at least at force maxima 1 and 2, and at number 3 only on the 10.6 kPa gels. Significance was established with $p < 0.05$, and all results are presented as mean $\pm$ SE of the mean.

## 3 Results

We have identified differences in morphology and forces applied by metastatic and benign breast cells during cell adhesion to an elastic PAM gels with varying stiffness. We have monitored the time-dependent changes in the cell morphology and in the traction forces applied by the cells during the adhesion process. Cells were imaged every hour up to 6.5 h, and results for high and low MP breast cancer cell lines were compared and contrasted with the control, benign breast cells.

We observe time-dependent changes in the morphologies of the adhering cells that differ depending on the metastatic potential of the cells. When seeded on gel with $E = 10.6 \pm 0.3$ kPa and following initial (biochemical) attachment, all the cells are round and exhibit different time-dependent changes in their morphologies (Fig. 2). The area of the benign cells increases with time, as the cells spread out on the gel, while the metastatic cells' areas remain unchanged (Fig. 2b). We observe a slight difference between the two metastatic cell lines, where the high MP cells cross-sections are typically smallest. We have also calculated the eccentricity and circularity (Fig. 2c) of the cell area, which, respectively, indicate cell shape deviations from roundness and the smoothness of the cell's perimeter. All the evaluated cell types exhibit similar, high values of smoothness at their perimeters (circularity close to unity), indicating few protrusions. As the benign cells increase their areas, their morphology becomes more elongated (more eccentric). In contrast, the high and low MP cells' areas remained unchanged on average, being mainly rounded throughout the experiment time, with the low MP cells being somewhat rounder and smoother. We also note the strain energy transmitted by the cells to the gels (Fig. 2d). We observe higher strain energy and reduction with time for the
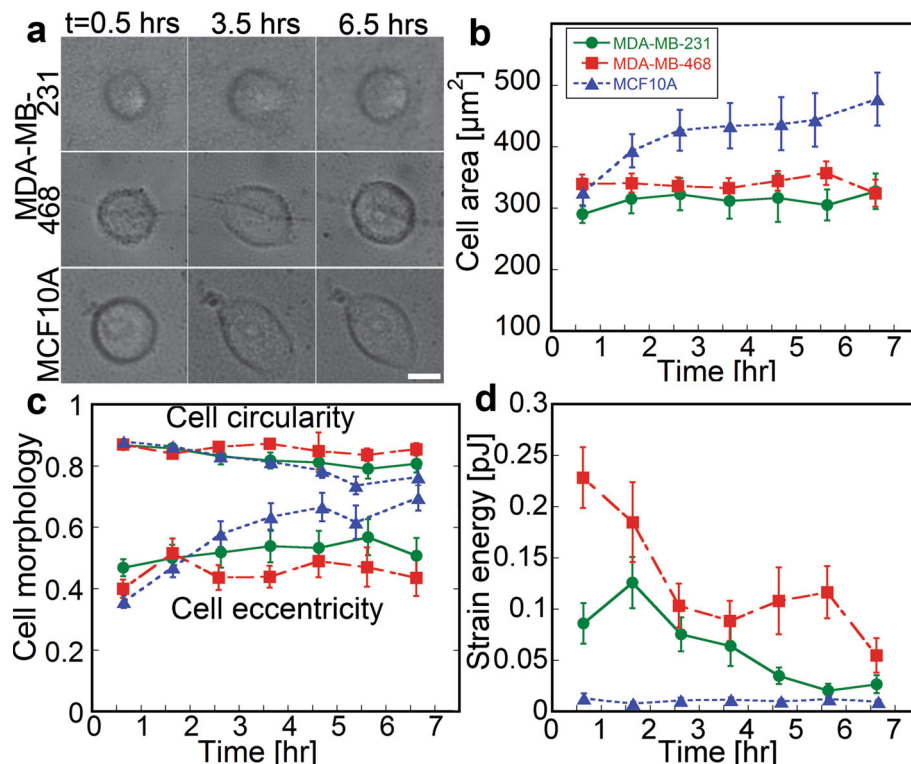
**Fig. 2** Average time-dependent cell morphologies on $10.6 \pm 0.3$ kPa PAM gel at $t = 0.5$, 3.5, and 6.5 h after seeding. **a** High MP breast cancer cells (MDA-MB-231) maintain a rounded morphology throughout the experiment. Low MP cells (MDA-MB-468) transiently change their morphology yet on average maintain a rounded shape. Benign breast cells (MCF 10A) spread out on the gel with time and become more elongated. *Scale bar* is 10 μm. **b** The area of the benign cells increases with time, while the cancer cells maintain a nearly constant area with time. **c** Cell morphology shown through the eccentricity and circularity.

The cell eccentricity increases as cells become elongated. In contrast, cell circularity (measure of surface smoothness) is constant and its value indicates nearly protrusion free cell-perimeters. The area and eccentricity of the high and low MP cancer cells are statistically different from benign cells ($p < 0.05$) starting at, respectively, 2.5 and 4.5 h after seeding. **d** Strain energy applied by the cells reduces with time for the metastatic cells, yet remains constant and low for the benign cells. Error bars are standard errors

metastatic cells, while the benign cells induce a constant and low strain energy.

Gel stiffness affects the cell morphology differently for the metastatic and the benign cells. We initially focus on the last time point, 6.5 h after cell seeding, and observe that the high MP and the low MP cells remain mainly rounded on PAM gels, regardless the gel stiffness (Fig. 3). In contrast, the benign cells are round on soft gels and are more elongated on stiffer gels ($E > 7$ kPa). To evaluate the differences in morphology, we have measured the cell areas and perimeters and have calculated the eccentricity and the circularity. Figure 3b shows that both of the metastatic breast cancer cell lines maintain nearly constant and similar attachment area on the evaluated gels, yet both exhibit a small increase in their adhesion area on gels with mid-range stiffness, i.e., Young's moduli of $4.3 \pm 0.3$ and $7.2 \pm 0.1$ kPa. Moreover, both high and low MP cells maintain constant eccentricity of about 0.5 (Fig. 3c), regardless of gel stiffness, representing the rounded shape. In contrast, we observe that

the benign cells increase their attachment area with gel stiffness and become more elongated on gels with $E > 7$ kPa; the eccentricity of the benign cells increases significantly with the gel stiffness ($p < 0.05$), while the circularity or surface roughness is independent of the gel stiffness at this time (not shown).

The smaller, rounded metastatic cancer cells are able to apply significantly larger traction forces to the gels than the larger area, spread out, benign cells (Fig. 4). We have measured the traction forces applied by the cells on the gel during the adhesion process as a function of the time-equivalent, local force maxima (see Sect. 2.6). The evaluated cells (15–20 single cells of each type and on each gel stiffness) exhibit a wide distribution of cell applied, time-dependent traction forces (Online Resource 3). Using the local force maxima approach to effectively normalize the different dynamic time-scales of the single cells, we observe statistically significant ($p < 0.05$) variation between the forces applied by each cell type (Fig. 4); similar trends are observed in the strain ener-
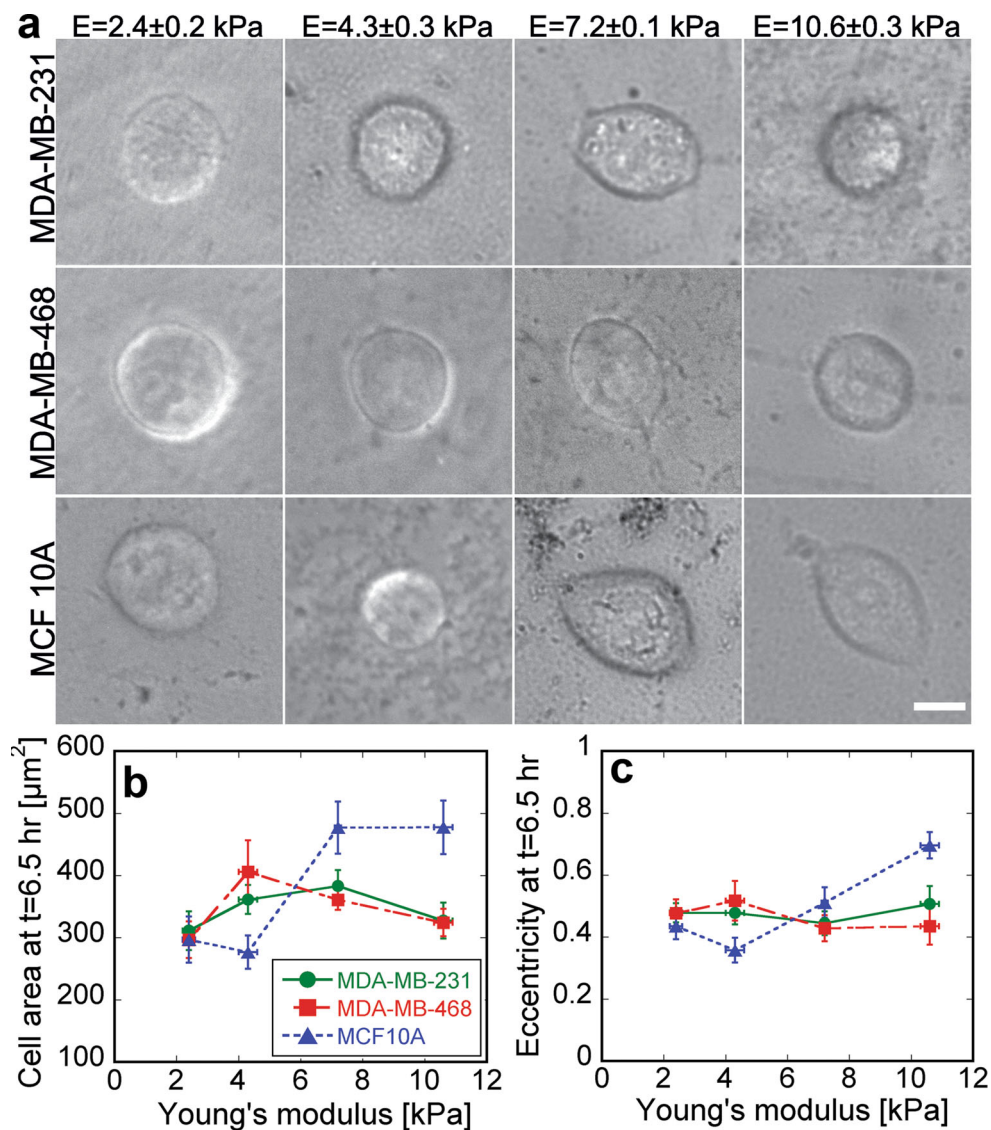
**Fig. 3** Cell morphologies on 2.4–10.6 kPa PAM gels at $t = 6.5$ h after seeding. **a** Cell images and **b** areas indicate that high MP (MDA-MB-231) and low MP (MDA-MB-468) cells are mainly round on the gels. Benign (MCF 10A) cells are round on soft gels ($E < 7$ kPa) and elongate on stiffer gels ($E > 7$ kPa). *Scale bar* is $10\,\mu$m. **c** The eccentricity quantifies changes in cell shape. *Error bars* are standard errors

gies applied by the cells (Online Resource 6). We observe that the metastatic breast cancer cell lines consistently apply larger total traction force than the benign cells. Interestingly, although differences in morphology of the low and high MP cells are small, the forces applied by the cells differ significantly. In addition, we observe that the low MP cells apply larger forces than high MP cells ($p < 0.05$) during adhesion to some gels. We also note that the traction forces reduce at higher values of local maxima number (i.e., longer times) for all cell types. This indicates that the total traction force amplitudes decrease with adhesion time, likely leading toward more stable morphologies and force distributions, as previously observed (Kraning-Rush et al. 2012).

## 4 Discussion

The metastatic breast cancer cells exhibit inherently different time- and gel-stiffness-dependent, mechanical interactions during the early stages of adhesion, as compared to benign control. We show that the cancer cells remain rounded and apply large traction forces to the underlying elastic gels with $E > 4$ kPa. In contrast, the benign cells spread out on the gel, increased their contact area, and concurrently applied smaller forces, likely to maintain their adhesion.

While remaining rounded, the metastatic cancer cells are able to apply significantly larger traction forces to the gel as compared to the benign cells (Fig. 4); those forces reduce

**Fig. 4** Average of peak, total traction force applied at local force maxima, correlated with time after seeding; low numbers are short times. The force amplitudes on all gel stiffnesses decrease with time. Only cells that applied measurable forces during at least 5 time points out of the total of 7 experimental time points were included, and all cells exhibited 3 local force maxima during the experiment time. **a** The cells apply the same amplitude of forces on the soft gel (2.4 kPa). **b**, **d** Low MP cells apply larger forces than high MP and both apply more force than benign cells, **c** high MP cells apply the highest forces. *Error bars* are standard errors
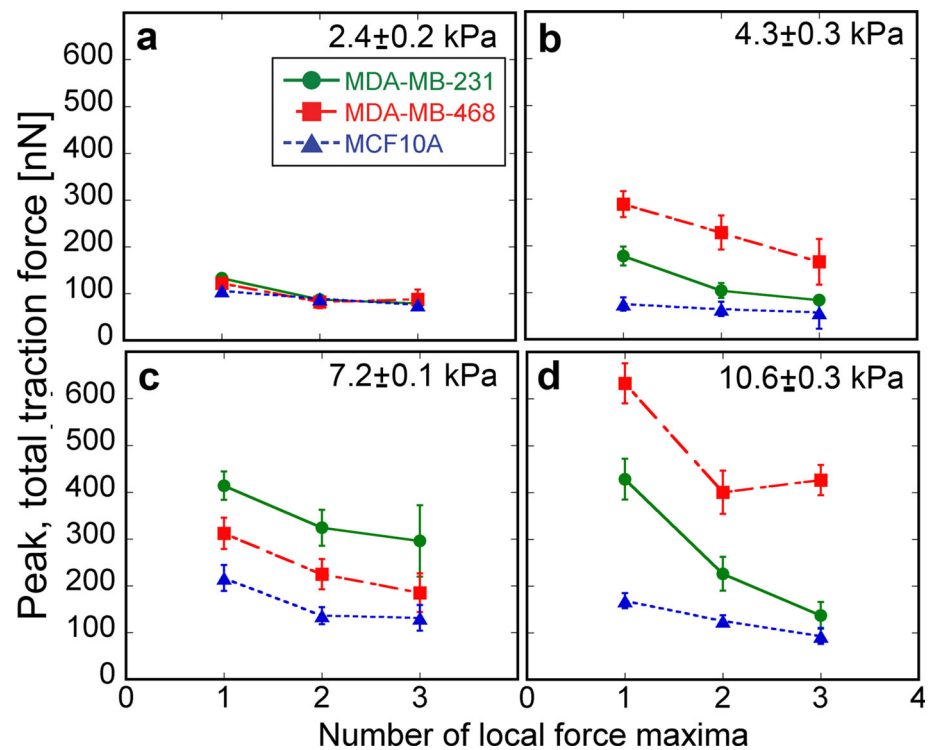


with time. Benign cells apply statistically smaller peak, total traction forces than the metastatic breast cancer cells, on all gels, except on the $2.4 \pm 0.2$ kPa gels. On those lowest stiffness gels, all the cells (benign and metastatic) apply similar, small traction forces (Fig. 3a) that do not significantly change with time; we had previously observed that on those gels many cells attempt indentation utilizing a combination of lateral and normal forces (Kristal-Muscal et al. 2013; Dvir et al. 2015; Kristal-Muscal et al. 2015). In contrast, on the stiffer gels, we observe that the metastatic cells apply a wide range of traction forces (100–600 nN), while forces applied by benign cells typically remain around 100 nN. Interestingly, on the $4.3 \pm 0.3$ and $10.6 \pm 0.3$ kPa PAM gels the low MP cells apply significantly larger traction forces than the high MP cells ($p < 0.05$), while on the $7.2 \pm 0.1$ kPa gel, the high MP cells apply larger traction forces. Concurrently, while the cells remain rounded, their areas change with time.

We observe that on the stiffer gels that were evaluated ($E > 4$ kPa), both the high MP and the low MP cells exhibit a decrease in the traction forces as the cell area on the gel increases (Online Resource 7); the cells remain round yet increase their contact area. In contrast, the benign cells maintain the force amplitude constant around 100 nN on all evaluated gels although the cells increase their area and become more eccentric on the stiffer gels; on the softest evaluated gel, the three cell lines are statistically indistinguishable.

Previous works have shown that more aggressive cells apply more force, at specific gel stiffness (Kraning-Rush et al. 2012). At the short times after seeding evaluated here,

we observe that depending on the gel stiffness sometimes the low MP cells apply more force. We have previously observed that fractions of the metastatic cells indent the gels, by forces other than solely in-plane traction (Kristal-Muscal et al. 2013; Dvir et al. 2015; Kristal-Muscal et al. 2015). The high MP cells typically exhibit a larger fraction of indenting cells, where in both cell types indentation decreases with gel stiffness; cells are unable to indent very stiff gels. This may suggest that the non-indenting subpopulation of the high MP cells evaluated here is somewhat weaker, on some gel stiffnesses, as compared to the corresponding subpopulation of the low MP cells; the non-indenting cells are typically more motile on the gel surface. The overall stronger traction forces applied by both of the metastatic cells and especially at shorter times likely facilitate, in an in vivo environment, rapid formation of new colonies, allowing the cells to rapidly modify their new environments and populate them.

We had previously observed a time-dependent reduction of the forces that lead to gel indentations (Kristal-Muscal et al. 2013) on soft gels (2.4 kPa) that was likely correlated with preservation of energy as the cells "recognize" through mechanotransduction that they are unable to penetrate the synthetic gels. A similar maturation of the interaction of the adhering cells with their substrate likely occurs here. Initially the adhering cells apply stronger forces to attach and to purposefully modify their environment, and as the cells establish their more stable contact with the impenetrable gel substrate, they require less force to maintain the contact. That is, the total traction forces are largest at the

shortest times after cell seeding and decrease as the cells form more stable connections. We observe that the forces measured at the longest times of our experiments are similar to the forces that have previously been measured 24 h after seeding (Kraning-Rush et al. 2012; Kristal-Muscal et al. 2015) on similar stiffness gels. This could again indicate stabilization of the cell adherence with time, although even at the longest timescale evaluated here, the metastatic cells still remain rounded (Kraning-Rush et al. 2012). Hence, the apparent "contact maturation" of the metastatic cells does not seem to require a change in the morphology of the metastatic breast cancer cells, in contrast to the benign cells.

To conclude, we note that monitoring the morphology and force application during the early stages of cell adhesion can be used to distinguish the benign from the metastatic cancer cells. We suggest that the rounded morphology maintained by the cancer cells likely enables them to apply more locally focused, stronger traction forces. We had also previously observed the same cells utilize the rounded morphology with a unique internal cell organization to apply combined lateral and normal forces and indent softer PAM gels (Raupach et al. 2007; Kristal-Muscal et al. 2013; Dvir et al. 2015); gels are impenetrable, and no chemoattractant was present. Concurrently to locally focusing the applied force, maintaining a rounded morphology may facilitate rapid detachment and migration of the cells if required. The larger forces applied by the evaluated metastatic cells likely facilitate their enhanced invasive and migratory capacity, as compared to the benign cells. While the generality of these phenomena would need to be verified using different cell types, the measurable parameters presented here may provide the basis for a quantitative and rapid approach to deliver a more general predictive prognosis for likelihood of metastases of tumor cell samples.

# References

Abuhattum S, Gefen A, Weihs D (2015) Ratio of total traction force to projected cell area is preserved in differentiating adipocytes. Integr Biol 7:1212–1217. doi:10.1039/c5ib00056d

Bershadsky AD, Balaban NQ, Geiger B (2003) Adhesion-dependent cell mechanosensitivity. Annu Rev Cell Dev Biol 19:677–695. doi:10.1146/annurev.cellbio.19.111301.153011

Boudou T, Ohayon J, Picart C et al (2009) Nonlinear elastic properties of polyacrylamide gels: implications for quantification of cellular forces. Biorheology 46:191–205. doi:10.3233/Bir-2009-0540

Butcher DT, Alliston T, Weaver VM (2009) A tense situation: forcing tumour progression. Nat Rev Cancer 9:108–122. doi:10.1038/Nrc2544

Butler JP, Tolic-Norrelykke IM, Fabry B, Fredberg JJ (2002) Traction fields, moments, and strain energy that cells exert on their surroundings. Am J Physiol Physiol 282:C595–C605

Christofori G (2006) New signals from the invasive front. Nature 441:444–450. doi:10.1038/nature04872

Cooney CA, Jousheghany F, Yao-Borengasser A et al (2011) Chondroitin sulfates play a major role in breast cancer metastasis: a role for CSPG4 and CHST11 gene expression in forming surface P-selectin ligands in aggressive breast cancer cells. Breast Cancer Res 13:R58. doi:10.1186/bcr2895

Cross SE, Jin YS, Rao J, Gimzewski JK (2007) Nanomechanical analysis of cells from cancer patients. Nat Nanotechnol 2:780–783. doi:10.1038/nnano.2007.388

Discher DE, Janmey P, Wang YL (2005) Tissue cells feel and respond to the stiffness of their substrate. Science 310:1139–1143. doi:10.1126/science.1116995

Dvir L, Nissim R, Alvarez-Elizondo MB, Weihs D (2015) Quantitative measures to reveal coordinated cytoskeleton-nucleus reorganization during in vitro invasion of cancer cells. New J Phys 17:43010

Gal N, Weihs D (2012) Intracellular mechanics and activity of breast cancer cells correlate with metastatic potential. Cell Biochem Biophys 63:199–209

Geiger B, Yamada KM (2011) Molecular architecture and function of matrix adhesions. Cold Spring Harb Perspect Biol 3:a005033. doi:10.1101/cshperspect.a005033

Goldstein D, Elhanan T, Aronovitch M, Weihs D (2013) Origin of active transport in breast-cancer cells. Soft Matter 9:7167–7173. doi:10.1039/c3sm50172h

Guck J, Schinkinger S, Lincoln B et al (2005) Optical deformability as an inherent cell marker for testing malignant transformation and metastatic competence. Biophys J 88:3689–3698. doi:10.1529/biophysj.104.045476

Ingber DE (2008) Tensegrity and mechanotransduction. J Bodyw Mov Ther 12:198–200. doi:10.1016/j.jbmt.2008.04.038

Kraning-Rush CM, Califano JP, Reinhart-King CA (2012) Cellular traction stresses increase with increasing metastatic potential. PLoS One 7:e32572. doi:10.1371/journal.pone.0032572

Kristal-Muscal R, Dvir L, Weihs D (2013) Metastatic cancer cells tenaciously indent impenetrable, soft substrates. New J Phys 15:35022. doi:10.1088/1367-2630/15/3/035022

Kristal-Muscal R, Dvir L, Schvartzer M, Weihs D (2015) Mechanical interaction of metastatic cancer cells with a soft gel. Procedia IUTAM 12:211–219. doi:10.1016/j.piutam.2014.12.023

Kumar S, Weaver VM (2009) Mechanics, malignancy, and metastasis: the force journey of a tumor cell. Cancer Metastasis Rev 28:113–127. doi:10.1007/s10555-008-9173-4

Lelievre SA, Weaver VM, Nickerson JA et al (1998) Tissue phenotype depends on reciprocal interactions between the extracellular matrix and the structural organization of the nucleus. Proc Natl Acad Sci USA 95:14711–14716

Levental I, Georges PC, Janmey PA (2007) Soft biological materials and their impact on cell function. Soft Matter 3:299–306. doi:10.1039/B610522j

Levental KR, Yu H, Kass L et al (2009) Matrix crosslinking forces tumor progression by enhancing integrin signaling. Cell 139:891–906. doi:10.1016/j.cell.2009.10.027

Lo CM, Wang HB, Dembo M, Wang YL (2000) Cell movement is guided by the rigidity of the substrate. Biophys J 79:144–152

Mak M, Reinhart-King CA, Erickson D (2013) Elucidating mechanical transition effects of invading cancer cells with a subnucleus-scaled microfluidic serial dimensional modulation device. Lab Chip 13:340–348. doi:10.1039/c2lc41117b

Mierke CT, Rosel D, Fabry B, Brabek J (2008) Contractile forces in tumor cell migration. Eur J Cell Biol 87:669–676. doi:10.1016/j.ejcb.2008.01.002

Mierke CT, Kollmannsberger P, Zitterbart DP et al (2010) Vinculin facilitates cell invasion into three-dimensional collagen matrices. J Biol Chem 285:13121–13130. doi:10.1074/jbc.M109.087171

Paszek MJ, Weaver VM (2004) The tension mounts: mechanics meets morphogenesis and malignancy. J Mammary Gland Biol Neoplasia 9:325–342. doi:10.1007/s10911-004-1404-x

Paszek MJ, Zahir N, Johnson KR et al (2005) Tensional homeostasis and the malignant phenotype. Cancer Cell 8:241–254. doi:10.1016/j.ccr.2005.08.010

Pelham RJ, Wang YL (1997) Cell locomotion and focal adhesions are regulated by substrate flexibility. Proc Natl Acad Sci USA 94:13661–13665

Peschetola V, Laurent VM, Duperray A et al (2013) Time-dependent traction force microscopy for cancer cells as a measure of invasiveness. Cytoskeleton 70:201–214. doi:10.1002/cm.21100

Rape AD, Guo WH, Wang YL (2011) The regulation of traction force in relation to cell shape and focal adhesions. Biomaterials 32:2043–2051. doi:10.1016/j.biomaterials.2010.11.044

Raupach C, Zitterbart DP, Mierke CT et al (2007) Stress fluctuations and motion of cytoskeletal-bound markers. Phys Rev E 76:11918. doi:10.1103/PhysRevE.76.011918

Ravdin PM, Siminoff LA, Davis GJ et al (2001) Computer program to assist in making decisions about adjuvant therapy for women with early breast cancer. J Clin Oncol 19:980–991

Ren ZX, Yu HB, Li JS et al (2015) Suitable parameter choice on quantitative morphology of A549 cell in epithelial–mesenchymal transition. Biosci Rep. doi:10.1042/BSR20150070

Ruppender NS, Merkel AR, Martin TJ et al (2010) Matrix rigidity induces osteolytic gene expression of metastatic breast cancer cells. PLoS One 5:e15451. doi:10.1371/journal.pone.0015451

Sidransky D (2002) Emerging molecular markers of cancer. Nat Rev Cancer 2:210–219. doi:10.1038/nrc755

Soine JR, Brand CA, Stricker J et al (2015) Model-based traction force microscopy reveals differential tension in cellular actin bundles. PLoS Comput Biol 11:e1004076. doi:10.1371/journal.pcbi.1004076

Vermolen FJ, Van Der Meijden RP, Van Es M et al (2015) Towards a mathematical formalism for semi-stochastic cell-level computational modeling of tumor initiation. Ann Biomed Eng 43:1680–1694. doi:10.1007/s10439-015-1271-1

Xiong Y, Rangamani P, Fardin M-A et al (2010) Mechanisms controlling cell size and shape during isotropic cell spreading. Biophys J 98:2136–2146. doi:10.1016/j.bpj.2010.01.059

Yeung T, Georges PC, Flanagan LA et al (2005) Effects of substrate stiffness on cell morphology, cytoskeletal structure, and adhesion. Cell Motil Cytoskelet 60:24–34. doi:10.1002/cm.20041

Zaman MH, Trapani LM, Siemeski A et al (2006) Migration of tumor cells in 3D matrices is governed by matrix stiffness along with cell-matrix adhesion and proteolysis. Proc Natl Acad Sci USA 103:10889–10894. doi:10.1073/pnas.0604460103